2022 IEEE International Instrumentation and Measurement Technology Conference (I2MTC) | 978-1-6654-8360-5/22/$31.00 ©2022 IEEE | DOI: 10.1109/I2MTC48687.2022.9806535

Monitoring of Seagrass Meadows Using Satellite Images and U-Net Convolutional Neural Network

Marco Scarpetta
Department of Electrical and Information Engineering
Polytechnic University of Bari
Bari, Italy
marco.scarpetta@poliba.it

Paolo Affuso
Department of Electrical and Information Engineering
Polytechnic University of Bari
Bari, Italy
p.affuso@studenti.poliba.it

Maddalena de Virgilio
Institute of Biosciences and Bioresources
National Research Council
Bari, Italy
maddalena.devirgilio@ibbr.cnr.it

Maurizio Spadavecchia
Department of Electrical and Information Engineering
Polytechnic University of Bari
Bari, Italy
maurizio.spadavecchia@poliba.it

Gregorio Andria
Department of Electrical and Information Engineering
Polytechnic University of Bari
Bari, Italy
gregorio.andria@poliba.it

Nicola Giaquinto
Department of Electrical and Information Engineering
Polytechnic University of Bari
Bari, Italy
nicola.giaquinto@poliba.it

***Abstract*—Seagrass meadows are a very important component of coastal ecosystems, but they are constantly threatened due to anthropic activities. An effective and frequent monitoring of seagrass meadows is therefore widely recognized as an urgent need for their conservation as well as to have an indicator of excessive anthropic pressure on marine ecosystems. This paper explores the use of a deep learning-based image segmentation model for the monitoring of marine seagrass meadows through satellite images. The model can perform a pixel-wise classification of the image, recognizing land, seawater, and seagrass meadows. A dataset of high-resolution satellite images of regions along the Apulian coastline was created and used as training dataset for the deep learning model. The classification performances of the model were then assessed using a set of test images and very promising results were obtained.**

Keywords—satellite monitoring, deep learning, convolutional neural network, seagrass, Posidonia oceanica

I. Introduction

It is widely recognized that human activities and climatic change are causing more and more transformations to seas, coasts and related ecosystems, bringing to the environment serious threats, which must be put under control. As a consequence, many techniques have been developed for the monitoring and modeling of coastal erosion [1]–[4], pollution and quality of water [5]–[11], population and health of marine colonial animals [12]–[14], and of size, biodiversity and distribution of seagrass meadows [15]–[18].

In this paper, we consider the monitoring of the marine meadows of *Posidonia oceanica* (L.) Delile, which constitutes an extremely important and productive coastal ecosystems. This plant, a source of carbon sequestration, is the largest producer of oxygen in the Mediterranean Sea, dispenses nutrients for the food chain of herbivores, feeds the trophic transfer to adjacent habitats, increases fishing, stabilizes sediments and counteracts coastal erosion. *P. oceanica* is also considered an excellent bioindicator of the health status of the surrounding marine ecosystems, as well as of the environmental and anthropogenic pressures that are causing its worrying regression in the Mediterranean Sea, particularly significant in the vicinity of the main urbanized areas and port structures [16], [19]–[23]. In fact, during the twentieth century and in particular since the 1940s, the loss of algae beds has been observed in various regions due to numerous factors: leakage of sediments and nutrients into the sea, extension of ports and piers, increase in impact of industry, construction, shipping, overfishing, dredging and mining, invasion of alien species, algal blooms, bottom trawling, climate change and ocean acidification [24]. In addition, in parallel with the prevalently anthropogenic disturbance of seagrasses, these ecosystems also exhibit a very slow and variable growth rate between species. Although the EU Habitats Directive [25] considers marine phanerogams among the priority habitats, and despite these having become one of the main protection objectives of the Mediterranean Sea, marine phanerogams are often not taken into consideration in management plans; the need for effective spatiotemporal monitoring strategies, however, is now widely recognized [26], [27].

Traditional monitoring e.g., using boats equipped with side scan sonars, underwater vehicles, scuba divers, etc., requires large resources and is inherently slow. This kind of monitoring activities were carried out in the past in Apulia Region, Italy. In 2006, the project "Inventory and Cartography of the Posidonia Meadows in the Maritime Compartments of Manfredonia, Molfetta, Bari, Brindisi, Gallipoli and Taranto" was carried out by COISPA [28]. The result of the project was a map of the *P. oceanica* meadows in Apulia's sea, differentiated by type e.g., on rock or on sand. The project also provided photos and descriptive videos of the different types of Posidonia meadows. Subsequently, in 2014, the "BIOMAP: Marine Bioconstructions in Puglia" project was developed by a consortium of Italian universities and public institutions [29]. One of the aims of the project was to map the marine biostructures, including *P. oceanica*, in Apulia's sea. More recently, other research activities on more limited areas have been completed, involving the monitoring of ten *P. oceanica* meadows in Apulia [15].

978-1-6654-8360-5/22/$31.00 ©2022 IEEE

An alternative approach to traditional monitoring would be to use publicly available aerial and satellite imagery data, along with machine learning and deep learning techniques. Currently available satellites for monitoring applications provide high-resolution images (up to 30 cm per pixel) of the whole world surface, updated with high frequency (revisit time up to 2–3 days). If these data are exploited in the most effective way, a large-scale spatiotemporal mapping and monitoring of marine plants can be achieved.

Previous studies have carried out research and analysis of seagrass meadows using satellite images. In [18], *P. oceanica* seagrass habitats in Aegean and Ionian Seas (in Greek territorial waters) were mapped using Copernicus Sentinel-2 multispectral images. A great number of Sentinel-2 pixels, having 10-m resolution, was collected. The pixels were relative to sea portions along the Greek coastline and contained seven different bands provided by Sentinel-2 satellites. The pixels were then classified using both information from high-resolution satellite images and knowledge from fieldwork activities. This dataset was therefore used to train a support vector machine (SVM) classifier, that was later used to classify larger areas of the Greek sea. A classification accuracy of 72% was found based on independent field data.

In this study, we aimed to develop an autonomous recognition and classification system of seagrass meadows present along the Apulian coastline. High resolution satellite images were used as input data for a deep learning-based image segmentation model. These models, typically based on convolutional neural networks (CNNs), have proved to be exceptionally effective for applications such as medical image analysis, traffic control systems, video surveillance, pedestrian detection for autonomous vehicles [30]. Here, an image segmentation model is used for the classification of regions in satellite images into three classes: land, seawater, and seagrass meadows. The model, trained and tested using high resolution satellite images, reached very good performances.

II. Methodology

A. Composition of the Satellite Imagery Dataset

A dataset of satellite images of limited regions along the Apulian coastline was created. The images were collected using the ArcGIS Pro software. In particular, the images were extracted from the "World Imagery" layer, that provided true-color images within 3–5 years of occurrent, typically, for most of the world. The images constituting the dataset were relative to the following eight locations:

- Pantanagianni–Pezze Morelli (Brindisi), image size: 768×512
- Castello di Santo Stefano (Monopoli, Bari), image size: 512×512
- Lido Accessibile Magna Grecia (Taranto), image size: 768×768
- Torre Testa (Brindisi), image size: 1024×768
- Lido Bruno (Taranto), image size: 1024×1024
- Penisola della Strea (Lecce), image size: 768×768
- Salina Vecchia (Brindisi), image size: 1792×2048
- Torre Rossa (Brindisi), image size: 2048×1280

The satellite images were manually labeled partitioning all their pixels into segments and assigning one of the following classes to each of them:

- Land (class 1)
- Seawater (class 2)
- Seagrass meadows (class 3)

As an example, one satellite image (of "Penisola della Strea") and the corresponding label are presented in Fig. 1. This image and the others composing the dataset were segmented by visual inspection, exploiting also the information provided by the available maps described in Section I. However, this manual labeling operation presented some limitations because it was not possible to know the real state of the seabed and its composition without carrying out in situ surveys. Anyway, the procedure developed in the study can be replicated using a more accurate dataset for actual spatiotemporal monitoring applications.

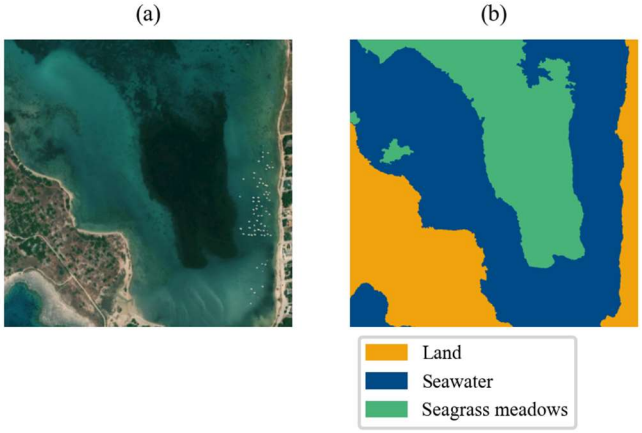

Fig. 1. Satellite image of "Penisola della Strea" (a). Segmented version of the satellite image (b).

The eight images were then fragmented into squared tiles of size 256×256. This is the size that the neural network for image segmentation accepts as input. A total of 152 tiles were obtained after fragmentation. Thirty-four of them were reserved for testing, taking at least 20% of tiles from each of the initial images. The remaining 118 tiles were used for training, instead.

The dataset was almost balanced, with 25.4%, 35.7% and 38.9% of pixels classified as land, seawater and seagrass meadows, respectively. The same percentage of pixels for each class was also preserved in the training and test sub-datasets. Since the topic of this study was dedicated to marine meadows, less regions of land were included in the dataset than regions of sea and seagrass meadows. Besides, land regions are easily distinguishable from the other two classes and in fact, as shown later, the unbalance was not detrimental to the classification performances of the neural network.

1) Data augmentation

The dataset of images reserved for training was augmented in order to increase the number of different samples used for training and hence improve the generalization properties of the neural network. The operations performed to generate the augmented dataset were the same for both the images and the

labels. In detail, the following operations were performed for each image:

- Random rotation, with an angle in the range 0°–360°
- Random horizontal and vertical shifts
- Random zoom in the range 90%–110%
- Random horizontal and vertical flip

The portions of images that remained empty after the augmentation procedure, were filled according to a "wrap" strategy i.e. by repeating the image and then selecting the pixels in the initial 256×256 tile region only. Sixteen augmented images were generated for each image in the starting dataset. The number of samples in the training dataset was therefore increased to 1888. Some examples of images after the augmentation process are presented in Fig. 2.

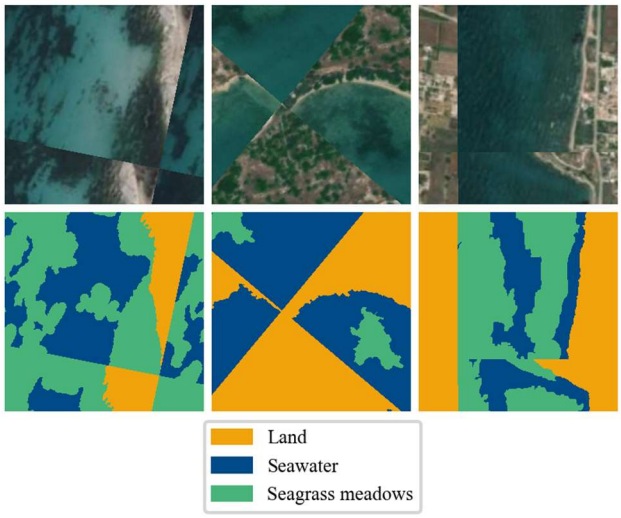

Fig. 2. Examples of augmented images (first row) and their corresponding labels (second row).

B. *Neural Network Model for Image Segmentation*

The aim of the neural network was to classify into the three defined categories all the pixels of the true-color images. Therefore, in this work, a supervised classification problem was addressed, using labels manually extracted from high spatial resolution true-color satellite images. The neural network architecture selected for the task is the U-Net convolutional neural network [31]. U-Net was initially proposed for biomedical image segmentation but was then used for general image segmentation tasks and became one the most widely used deep learning models for image segmentation. One advantage of the U-Net model is that it can be trained using few labeled samples, obtaining good results [30].

The basic structure of a U-net architecture consists of two paths. The first one is the contraction path that serves as encoder. It produces a lower resolution representation of the input image, containing its contextual semantic information. Each block in the contraction path consists of two successive 3×3 convolutions followed by a Rectified Linear Unit (ReLU) activation function and a max-pooling layer. This base sequence is repeated several times, doubling the number of convolutional kernels at each step. The expansion path, instead, synthetizes the segmented version of the starting image using the information provided by the blocks of the contraction path. The expansion path is symmetrical to the contraction path and, therefore, it consists of convolutional layers with a decreasing number of kernels followed by up-sampling layers. One important aspect of the U-Net architecture is that the outputs of the blocks in the contraction path are concatenated with the inputs of the blocks in the expansion path.

The standard U-Net model was modified to better fit this specific application. The main difference from the standard U-Net model was the addition of Dropout layers between the pairs of consecutive convolutional layers. Dropout was proved to help neural networks generalize and prevent overfitting [32], which is crucial when a small number of training samples is available. Other hyperparameters of the network, such as the number of kernels in convolutional layers and their size have not been further optimized. A detailed scheme of the neural network used in this study is depicted in Fig. 3. The input of the CNN was a 256×256 RGB image, corresponding to a tensor with shape 256×256×3. The contraction path was composed of five blocks, with convolutional layers containing an increasing number of kernels, from 16 to 256. The expansion path was symmetrical to the contraction path and, hence, it was terminated by convolutional layers containing 16 kernels. The last layer of the network was a 1×1 convolutional layer with three kernels, as the number of classes in labels. The Softmax activation was used in this layer.

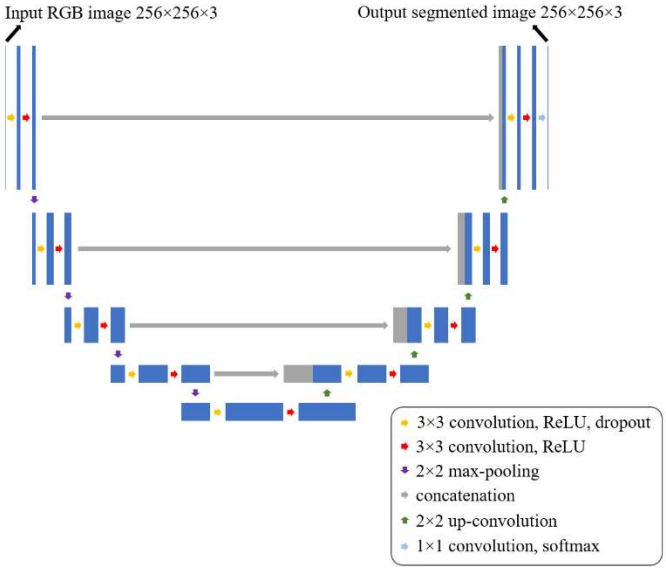

Fig. 3. Architecture of the U-net CNN used for image segmentation.

C. *Training of the Neural Network Model*

The neural network model was trained using the dataset of RGB satellite images described in Section II.A. The only preprocessing operation performed before the training was the normalization of the RGB images relative to the range 0–1. The categorical cross-entropy was used as loss function:

$$L = -\frac{1}{N_b \cdot N_w \cdot N_h \cdot N_c} \sum_{n=1}^{N_b} \sum_{i=1}^{N_w} \sum_{j=1}^{N_h} \sum_{k=1}^{N_c} y_{i,j,k}^{(n)} \log \hat{y}_{i,j,k}^{(n)}$$

where N_b was the batch size used in training, $N_x = N_y = 256$ were the width and height of the images, N_c was the number of classes, $y^{(n)}$ were the one-hot-encoded labels, $\hat{y}^{(n)}$ were the outputs of the Softmax operation performed by the last layer of the neural network. The one-hot encoded labels were defined as:

$$y_{i,j,k}^{(n)} = \begin{cases} 1, & \text{if class of pixel } i,j \text{ is } k \\ 0, & \text{otherwise} \end{cases}$$

The loss function was minimized using the Adam optimizer [33]. During training, the learning rate was decreased according to an exponential decay that caused it to halve each 20 epochs. The batch size was set to $N_b = 8$ and the model was trained for 100 epochs.

The CNN was implemented in Python using the Tensorflow framework [34]. The training procedure was performed using an NVIDIA RTX 3060 GPU.

III. Results and Discussion

The neural network model was trained as described in Section II.C. A fraction of the augmented training dataset, corresponding to 20% of the samples, was used for validation during the training process. Intersection over Union (IoU) was the metric selected to assess the performances of the model in the segmentation task. This metric is very common in image segmentation tasks because it evaluates the overlapping between predicted and ground-truth regions independently on their size, and hence does not produce misleading results when working with unbalanced datasets, such as e.g., the accuracy metric can do.

The training process was summarized in the diagrams of Fig. 4, where the loss function and the IoU metric were plotted versus epochs, for both the training and validation datasets. As can be seen, the mean IoU was plateauing above 0.9 at the end of the training, and no significant overfitting was detectable.

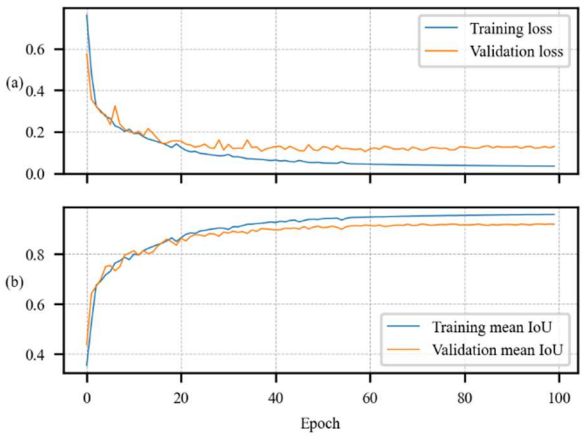

Fig. 4. Loss function variation during the training process (a). Mean IoU variation during the training process (b).

After the training process, the model's performances were assessed using the test dataset of thirty-four 256×256 tiles. Since the test tiles were selected in contiguous regions, it was possible to recompose them in the bigger images depicted in Fig. 5.

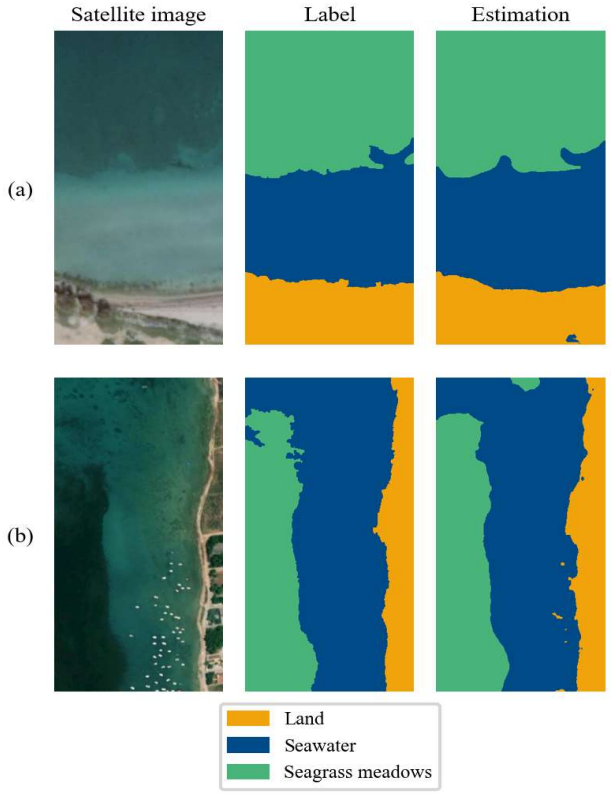

Fig. 5. Segmentation result obtained for the test tiles of satellite image of "Lido Accessibile Magna Grecia" (a) and "Penisola della Strea" (b).

The IoU score obtained for each of the three classes and the global mean IoU are reported in Table I. As expected, the land regions were recognized more easily, but good classification results were also obtained for sea and seagrass meadows, as is also possible to see from Fig. 5.

TABLE I. Results of Performances Assessment on the Test Dataset

Class	IoU
Land	0.98
Seawater	0.80
Seagrass meadows	0.83
Mean	0.87

The overall classification accuracy was 92%. These results can be considered quite satisfactory, considering that in the work [18] the observed overall accuracy of *P. Oceanica* was about 72%.

IV. Conclusions

In this study, a method based on the usage of a deep-learning image segmentation model was proposed for the analysis of satellite images for seagrass meadows monitoring applications. The dataset for training the convolutional neural network model was created starting from high-resolution satellite images. Those images were pixel-wise labeled based on visual inspection and information from previous mappings derived from fieldwork

studies. The classification performances of the model were assessed using a sub-set of the labeled images. The results showed that the model was able to classify the satellite images with good accuracy and the proposed technique can therefore be effectively used for spatiotemporal monitoring of seagrass meadows.

Future implementations of this technique involve the improvement of the dataset both in qualitative and quantitative terms. Besides being desirable, as usual, a larger number of labeled images, it is also important to validate and improve the labeling, by more detailed in situ analysis of the underwater biostructures (a costly and demanding activity, which, however, can be made more accurate and affordable using clearer images taken by drones [14], [35]). The present work, however, provides the methodology for a fast, low cost and low impact monitoring of marine biostructures in space and in time, and practical results for the Apulia region in Italy, following up previous studies in the same area.

REFERENCES

[1] F. Adamo, C. De Capua, P. Filianoti, A. M. L. Lanzolla, and R. Morello, "A coastal erosion model to predict shoreline changes," *Measurement*, vol. 47, pp. 734–740, Jan. 2014, doi: 10.1016/j.measurement.2013.09.048.

[2] L. Mentaschi, M. I. Vousdoukas, J.-F. Pekel, E. Voukouvalas, and L. Feyen, "Global long-term observations of coastal erosion and accretion," *Sci Rep*, vol. 8, no. 1, Art. no. 1, Aug. 2018, doi: 10.1038/s41598-018-30904-w.

[3] A. Capolupo *et al.*, "An Interactive WebGIS Framework for Coastal Erosion Risk Management," *Journal of Marine Science and Engineering*, vol. 9, no. 6, Art. no. 6, Jun. 2021, doi: 10.3390/jmse9060567.

[4] A. Spinosa, A. Ziemba, A. Saponieri, V. D. Navarro-Sanchez, L. Damiani, and G. E. Serafy, "Automatic Extraction of Shoreline from Satellite Images: a new approach," in *2018 IEEE International Workshop on Metrology for the Sea; Learning to Measure Sea Health Parameters (MetroSea)*, Oct. 2018, pp. 33–38. doi: 10.1109/MetroSea.2018.8657864.

[5] F. Adamo, F. Attivissimo, C. G. C. Carducci, and A. M. L. Lanzolla, "A Smart Sensor Network for Sea Water Quality Monitoring," *IEEE Sensors Journal*, vol. 15, no. 5, pp. 2514–2522, May 2015, doi: 10.1109/JSEN.2014.2360816.

[6] F. Attivissimo, C. G. C. Carducci, A. M. L. Lanzolla, A. Massaro, and M. R. Vadrucci, "A Portable Optical Sensor for Sea Quality Monitoring," *IEEE Sensors Journal*, vol. 15, no. 1, pp. 146–153, Jan. 2015, doi: 10.1109/JSEN.2014.2340437.

[7] F. Adamo *et al.*, "GeoLab, a measurement system for the geotechnical characterization of polluted submarine sediments," *Measurement*, vol. 127, pp. 335–347, Jan. 2018, doi: 10.1016/j.measurement.2018.06.001.

[8] F. Cotecchia *et al.*, "A geo-chemo-mechanical study of a highly polluted marine system (Taranto, Italy) for the enhancement of the conceptual site model," *Sci Rep*, vol. 11, no. 1, Art. no. 1, Feb. 2021, doi: 10.1038/s41598-021-82879-w.

[9] S. Angelliaume *et al.*, "SAR Imagery for Detecting Sea Surface Slicks: Performance Assessment of Polarization-Dependent Parameters," *IEEE Transactions on Geoscience and Remote Sensing*, vol. 56, no. 8, pp. 4237–4257, Aug. 2018, doi: 10.1109/TGRS.2018.2803216.

[10] K. Nazirova and O. Lavrova, "Monitoring of Marine Pollution in the Gulf of Lion Based on Remote Sensing Data," in *2018 OCEANS - MTS/IEEE Kobe Techno-Oceans (OTO)*, May 2018, pp. 1–5. doi: 10.1109/OCEANSKOBE.2018.8559272.

[11] A. Spinosa, A. Ziemba, A. Saponieri, L. Damiani, and G. El Serafy, "Remote Sensing-Based Automatic Detection of Shoreline Position: A Case Study in Apulia Region," *Journal of Marine Science and Engineering*, vol. 9, no. 6, Art. no. 6, Jun. 2021, doi: 10.3390/jmse9060575.

[12] G. Chimienti, A. Di Nisio, A. M. L. Lanzolla, G. Andria, A. Tursi, and F. Mastrototaro, "Towards Non-Invasive Methods to Assess Population Structure and Biomass in Vulnerable Sea Pen Fields," *Sensors*, vol. 19, no. 10, Art. no. 10, Jan. 2019, doi: 10.3390/s19102255.

[13] G. Chimienti, A. Di Nisio, and A. M. L. Lanzolla, "Size/Age Models for Monitoring of the Pink Sea Fan Eunicella verrucosa (Cnidaria: Alcyonacea) and a Case Study Application," *Journal of Marine Science and Engineering*, vol. 8, no. 11, Art. no. 11, Nov. 2020, doi: 10.3390/jmse8110951.

[14] A. M. Dujon *et al.*, "Machine learning to detect marine animals in UAV imagery: effect of morphology, spacing, behaviour and habitat," *Remote Sensing in Ecology and Conservation*, vol. 7, no. 3, pp. 341–354, 2021, doi: 10.1002/rse2.205.

[15] M. de Virgilio, S. Cifarelli, P. de Gennaro, G. Garofoli, and B. Degryse, "A first attempt of citizen science in the genetic monitoring of a Posidonia oceanica meadow in the Italian Southern Adriatic Sea," *Journal for Nature Conservation*, vol. 56, p. 125826, Aug. 2020, doi: 10.1016/j.jnc.2020.125826.

[16] L. Telesca *et al.*, "Seagrass meadows (Posidonia oceanica) distribution and trajectories of change," *Sci Rep*, vol. 5, no. 1, p. 12505, Jul. 2015, doi: 10.1038/srep12505.

[17] D. Traganos and P. Reinartz, "Mapping Mediterranean seagrasses with Sentinel-2 imagery," *Mar Pollut Bull*, vol. 134, pp. 197–209, Sep. 2018, doi: 10.1016/j.marpolbul.2017.06.075.

[18] D. Traganos, B. Aggarwal, D. Poursanidis, K. Topouzelis, N. Chrysoulakis, and P. Reinartz, "Towards Global-Scale Seagrass Mapping and Monitoring Using Sentinel-2 on Google Earth Engine: The Case Study of the Aegean and Ionian Seas," *Remote Sensing*, vol. 10, no. 8, p. 1227, Aug. 2018, doi: 10.3390/rs10081227.

[19] C. F. Boudouresque, N. Mayot, and G. Pergent, "The outstanding traits of the functioning of the Posidonia oceanica seagrass ecosystem," *Biologia Marina Mediterranea*, vol. 13, no. 4, pp. 109–113, 2006.

[20] G. Casazza, C. Lopez Royo, and C. Silvestri, "Seagrass as key coastal ecosystems: an overview of the recent EU WFD requirements and current applications," *Biologia Marina Mediterranea*, vol. 13, no. 4, pp. 189–193, 2006.

[21] R. J. Orth *et al.*, "A Global Crisis for Seagrass Ecosystems," *BioScience*, vol. 56, no. 12, pp. 987–996, Dec. 2006, doi: 10.1641/0006-3568(2006)56[987:AGCFSE]2.0.CO;2.

[22] M. Montefalcone, "Ecosystem health assessment using the Mediterranean seagrass Posidonia oceanica: A review," *Ecological Indicators*, vol. 9, no. 4, pp. 595–604, Jul. 2009, doi: 10.1016/j.ecolind.2008.09.013.

[23] N. Marbà, C. M. Duarte, J. Cebrián, M. E. Gallegos, B. Olesen, and K. Sand-Jensen, "Growth and population dynamics of Posidonia oceanica on the Spanish Mediterranean coast: elucidating seagrass decline," *Marine Ecology Progress Series*, vol. 137, no. 1/3, pp. 203–213, 1996.

[24] M. Barange, J. G. Field, R. P. Harris, E. E. Hofmann, R. I. Perry, and F. Werner, Eds., *Marine Ecosystems and Global Change*. Oxford: Oxford University Press, 2010. doi: 10.1093/acprof:oso/9780199558025.001.0001.

[25] *Council Directive 92/43/EEC of 21 May 1992 on the conservation of natural habitats and of wild fauna and flora*, vol. OJ L. 1992. Accessed: Dec. 02, 2021. [Online]. Available: http://data.europa.eu/eli/dir/1992/43/oj/eng

[26] A. Grech *et al.*, "A comparison of threats, vulnerabilities and management approaches in global seagrass bioregions," *Environ. Res. Lett.*, vol. 7, no. 2, p. 024006, Apr. 2012, doi: 10.1088/1748-9326/7/2/024006.

[27] C. M. Duarte, W. C. Dennison, R. J. W. Orth, and T. J. B. Carruthers, "The Charisma of Coastal Ecosystems: Addressing the Imbalance," *Estuaries and Coasts: J CERF*, vol. 31, no. 2, pp. 233–238, Apr. 2008, doi: 10.1007/s12237-008-9038-7.

[28] CoNISMa Consorzio nazionale interuniversitario per le scienze del mare, *Inventario e cartografia delle praterie di Posidonia nei compartimenti marittimi di manfredonia, Molfetta, Bari, Brindisi, Gallipoli e Taranto*. Crisma, 2006. [Online]. Available: https://books.google.it/books/about/Inventario_e_cartografia_delle_praterie.html?id=KiDGoAEACAAJ

[29] "BIOMAP: Biocostruzioni marine in Puglia - Marine bioconstructions in Apulia (in Italian)." http://www.sit.puglia.it/portal/portale_rete_ecologica/biomap

[30] S. Minaee, Y. Y. Boykov, F. Porikli, A. J. Plaza, N. Kehtarnavaz, and D. Terzopoulos, "Image Segmentation Using Deep Learning: A Survey,"

IEEE Transactions on Pattern Analysis and Machine Intelligence, pp. 1–1, 2021, doi: 10.1109/TPAMI.2021.3059968.

[31] O. Ronneberger, P. Fischer, and T. Brox, "U-Net: Convolutional Networks for Biomedical Image Segmentation," in *Medical Image Computing and Computer-Assisted Intervention – MICCAI 2015*, Cham, 2015, pp. 234–241. doi: 10.1007/978-3-319-24574-4_28.

[32] N. Srivastava, G. Hinton, A. Krizhevsky, I. Sutskever, and R. Salakhutdinov, "Dropout: A Simple Way to Prevent Neural Networks from Overfitting," p. 30.

[33] D. P. Kingma and J. Ba, "Adam: A Method for Stochastic Optimization," *arXiv:1412.6980 [cs]*, Dec. 2014, Accessed: Jun. 28, 2019. [Online]. Available: http://arxiv.org/abs/1412.6980

[34] M. Abadi *et al.*, "TensorFlow: Large-Scale Machine Learning on Heterogeneous Distributed Systems," *arXiv:1603.04467 [cs]*, Mar. 2016, Accessed: Dec. 09, 2021. [Online]. Available: http://arxiv.org/abs/1603.04467

[35] A. Di Nisio, F. Adamo, G. Acciani, and F. Attivissimo, "Fast Detection of Olive Trees Affected by Xylella Fastidiosa from UAVs Using Multispectral Imaging," *Sensors*, vol. 20, no. 17, Art. no. 17, Jan. 2020, doi: 10.3390/s20174915.